CORRELATION ANALYSIS BETWEEN PARK LANDSCAPE AND URBAN THERMAL ENVIRONMENT BASED ON IMPROVED MSRN2 ALGORITHM

HUA, Y.

School of Art and Design, Huaiyin Institute of Technology, Huai'an 223001, China
(e-mail: huaerfashi@163.com)

(Received 10th Jul 2025; accepted 14th Nov 2025)

Abstract. With the acceleration of urbanization and the intensification of urban heat island effect, traditional remote sensing methods have the problem of insufficient multi-scale feature capture when finely analyzing the connection between thermal environment and landscape elements. To address this issue, an improved multi-scale residual network 2 algorithm is proposed, which introduces a texture color dual branch feature extraction module and attention mechanism to optimize the dynamic fusion ability of multi-source remote sensing data, and combines the cellular Markov model to predict the spatiotemporal evolution of urban thermal environment, to explore the correlation between park landscape and thermal environment. The experimental results show that the improved multi-scale residual network 2 algorithm has a feature extraction accuracy of up to 0.98, with an efficiency improvement of about 60% compared to traditional models, which is a significant enhancement. In addition, the overall error of the cellular Markov model for thermal environment prediction is less than 5%. Correlation analysis shows that the degree of fragmentation in park landscapes is significantly correlated with the expansion of high-temperature areas, and the heat island effect exhibits a growing tendency. The research verifies the effectiveness of the improved algorithm and prediction model, providing scientific basis and technical support for optimizing urban green space planning and alleviating thermal environment problems.
Keywords: *park, hot environment, multi-scale residual network 2, cellular Markov model, convolutional neural network*

Introduction

As global urbanization intensifies, the urban thermal environment has emerged as a critical issue impacting the environment and sustainable development of cities (Kisamba and Li, 2023). The urban heat island effect (HIE) not only results in heightened energy utilization and worsening air pollution, but also directly threatens the health and ecological security of urban residents. In this context, urban green space landscapes, especially park systems, serve as important ecological regulation carriers. The study of the correlation between spatial layout, vegetation coverage, landscape structure characteristics, and thermal environment provides key scientific basis for mitigating the HIE (Said et al., 2024; Satalkar et al., 2024). However, traditional remote sensing interpretation methods have problems such as insufficient spatial resolution and limited ability to capture multi-scale features in the fine correlation analysis between thermal environment and landscape elements, which hinders the ability to satisfy accurate modeling in complex urban environments (Mustaquim and Islam, 2025). In recent years, deep learning technology has opened up novel avenues for remote sensing image analysis and environmental modeling. The Multi-scale Residual Network (MSRN) has demonstrated significant advantages in the field of image super-resolution reconstruction due to its multi-level feature fusion capability. Although the traditional MSRN algorithm has the ability to extract multi-scale features, it cannot explore the impact of landscape on thermal environment in the correlation analysis between complex urban landscapes and thermal environments (Atef et al., 2024; Abdelkarim, 2025). This method has

http://www.aloki.hu ● ISSN 1589 1623 (Print) ● ISSN 1785 0037 (Online)
DOI: http://dx.doi.org/10.15666/aeer/2401_353374

insufficient accuracy in capturing subtle features of highly heterogeneous landscape elements, making it difficult to fully analyze the nonlinear relationship between landscape spatial structure and surface temperature. Moreover, the original model lacks dynamic adaptability in cross modal feature fusion of multi-source remote sensing data, which can easily lead to the loss or redundancy of important environmental information (Simon et al., 2023). Therefore, with the aim of examining the interplay between urban park landscapes and thermal environments, a texture color dual branch feature extraction (FE) module was introduced to optimize the sensitivity of the network to key landscape factors. The MSRN2 algorithm was proposed for FE of urban park landscapes. Meanwhile, the study employed the Cellular Automata-Markov (CA-Markov) model to analyze the changes in urban surface temperature for prediction, to investigate the relationship between urban park landscapes and thermal environments.

The innovation of the research lies in proposing an improved MSRN2 algorithm, which embeds attention mechanism and adaptive feature selection module to achieve dynamic feature fusion of multi-source remote sensing data, significantly improving the ability to finely analyze heterogeneous elements of park landscapes. The main contribution of the research is to provide quantifiable decision support for optimizing urban green space allocation, promote innovation in the application paradigm of deep learning technology in ecological effect assessment, and have important practical value for alleviating the HIE and promoting urban sustainable development.

Related works

Residual Network (ResNet) is a type of deep learning method. Hou et al. (2023) proposed a hybrid residual and weak form loss combined pre activation network structure to address the difficulty of training traditional deep learning methods in elliptical interface problems. The results showed that this method exhibited high accuracy and robustness in both two-dimensional regular and irregular interface problems, as well as in the calculation of protein solvation free energy (Hou et al., 2023). Lewandowski and Paffenroth (2023) proposed a class of autoencoder training methods to shape feature residuals in response to the challenges of zero day attacks and data volume growth in network intrusion detection. The results indicated that autoencoder feature residuals could not only replace the original input feature set, but also provide the same or higher classification performance (Lewandowski and Paffenroth, 2023). Bian (2024) proposed a style loss and content loss guidance method based on a dual channel convolutional network to address the low efficiency of manual segmentation in landscape painting style transfer and FE. Through multi-layer feature map matching and decoder reconstruction layer by layer, effective extraction and control of features such as lines and textures can be achieved. The results showed that this method improved the transfer of landscape painting image style and FE while maintaining the traditional Chinese painting style (Bian, 2024). FE is an effective method for analyzing the landscape of urban parks. Hu et al. (2025) proposed a style transfer network based on Swin Transformer to tackle the problems of semantic loss and insufficient generation quality in the transfer of Chinese painting styles. The results showed that SSTR outperformed StyTr2 in terms of style loss and detail preservation on COCO and landscape painting datasets, effectively improving the quality and realism of Chinese landscape painting style transfer (Hu et al., 2025). Li (2023) proposed a method based on contour wave transformation to tackle the problem of insufficient accuracy and robustness in extracting texture features from landscape design images. The results showed that the accuracy of the algorithm was nearly 90%

http://www.aloki.hu ● ISSN 1589 1623 (Print) ● ISSN 1785 0037 (Online)
DOI: http://dx.doi.org/10.15666/aeer/2401_353374

when there were only 100 feature points, and it continued to improve with the increase of feature points, demonstrating better robustness and stability than other algorithms. It was suitable for FE and quality evaluation under various image distortions (Li, 2023). The existing landscape FE methods mainly distinguish urban landscape features from other similar areas in terms of color and texture of the target area.

CA-Markov is an effective land spatial situation prediction model. Jayabaskaran and Das (2023) proposed a spatiotemporal analysis method for predicting land use/cover changes and future trends in the Ranipet area, and used the CA-Markov model for simulation. The results showed that the CA-Markov model had higher prediction accuracy, with a kappa index of 82.6% and 76.2% for land use/cover change in 2029 and 2080, respectively, establishing a scientific grounding for regional land management (Jayabaskaran and Das, 2023). Solaimani and Darvishi (2024) proposed using CA-Markov to predict land use changes in the Urmia Lake Basin. The results showed that agricultural land and built-up areas would continue to increase, while vegetation and water area would further decrease. The Kappa coefficients of the CA-Markov model were 89.89% and 87.09%, respectively, providing a reliable basis for regional land use management (Solaimani and Darvishi, 2024). Luan et al. (2023) employed the CA-Markov model to analyze and predict the spatiotemporal evolution of land use in response to the changes in ecological environment and landscape pattern in Hohhot during the urbanization process. The results showed that between 2000 and 2020, there was a decrease in arable land, an increase in artificial surfaces, and a decline in habitat quality. Simulations in 2030 showed that this trend would continue. The research provided a scientific basis for future urban planning and management (Luan et al., 2023). Chen et al. (2023) proposed a method using Landsat remote sensing data and CA-Markov model for dynamic evaluation and prediction of the ecological environment quality decline caused by rapid urbanization in Yining City. The results showed that greening and humidity had a positive impact on ecology, while dryness and high temperature (HT) have a negative impact (Chen et al., 2023). Pouriyeh (2023) proposed a method using artificial neural networks and CA-Markov models to model land use changes in central Iran from 1991 to 2021. The results showed that future urban development would lead to the transformation of mountainous areas, wastelands, gardens, and farmland, with cities expanding to barren lands and mountainous areas, increasing the risk of floods (Pouriyeh, 2023). The existing land spatial situation prediction models mainly used Markov models. Although this model could effectively predict the changes in urban spatial land use, it could not intuitively present spatial distribution.

In summary, existing FE methods, especially those based on deep ResNets, often fail to effectively combine multi-scale environmental factors with landscape features, resulting in insufficient sensitivity to heterogeneous urban elements. The study proposes an improved MSRN2 algorithm that combines a dual branch texture color FE module and attention mechanism, enhancing multi-scale feature fusion and sensitivity to key heat related landscape factors. Combined with the CA Markov model used for spatiotemporal prediction of thermal environment evolution, this integrated method can more finely analyze the correlation between park landscape structure and urban heat distribution. However, the proposed method may still be limited by the resolution of land satellite images, which may restrict the detection of microscale landscape features.

Methods and materials

Urban landscape FE based on improved MSRN2 algorithm

ResNet is a deep learning model architecture that has made breakthrough progress in fields such as image recognition and has become one of the cornerstones of modern deep learning. MRSN is a type of ResNet that extracts features at different scales by designing convolution kernels or pooling operations at different scales in the network (Gloire et al., 2023). The landscape of urban parks is mainly distinguished by texture and color in remote sensing images. MRSN is mainly used to extract regional features at different scales, and its FE effect on urban park landscapes is poor. Therefore, an improved MRSN model with dual branches of texture and color, namely MRSN2, was designed, and the comprehensive framework of the model is shown in *Figure 1*.

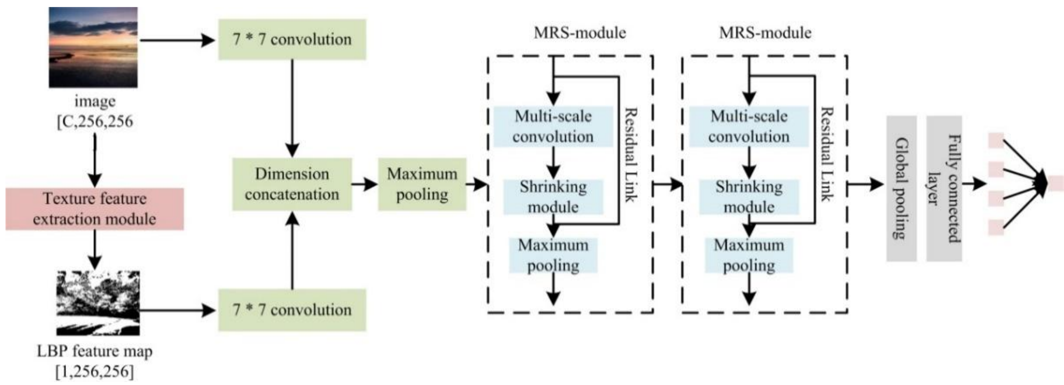

Figure 1. *Comprehensive framework of MSRN 2 model*

As presented in *Figure 1*, the research design model consists of two branch structures combined with feature fusion and classification structures. The two-branch structure corresponds to the novel texture-color dual-branch FE module, which is a key innovation of the proposed model. The branch structure corresponds to the texture color FE module, which adopts a two branch structure for arrangement. Feature fusion is processed by a multi-scale residual shrinkage module, another newly introduced component designed to enhance feature refinement and denoising capability, while classification is handled by a classification layer (Zui, 2024; Chen et al., 2025). This model adopts a bimodal feature decoupling learning framework: in the color processing pathway, a deep network based on improved ResNet (cardinality=32) is constructed, and spectral invariant features are extracted through grouped convolution; In the texture processing pathway, an LBP Transformer hybrid module, which is a novel combination designed to capture both local texture patterns and global contextual associations, is designed to capture the underlying texture using local binary patterns and enhance global texture associations through Transformer attention mechanism. The feature fusion stage introduces a learnable dynamic gating mechanism to achieve adaptive spatial alignment and scale normalization of features. The texture FE module is shown in *Figure 2*.

As presented in *Figure 2*, the texture FE part consists of spatial attention, color space transformation, and LBP operator. This integrated structure forms the core of the novel texture branch. The spatial attention mechanism can enhance the calculation of image features, and the calculation of image features enhanced by the attention mechanism is shown in *Equation (1)*.

http://www.aloki.hu ● ISSN 1589 1623 (Print) ● ISSN 1785 0037 (Online)
DOI: http://dx.doi.org/10.15666/aeer/2401_353374

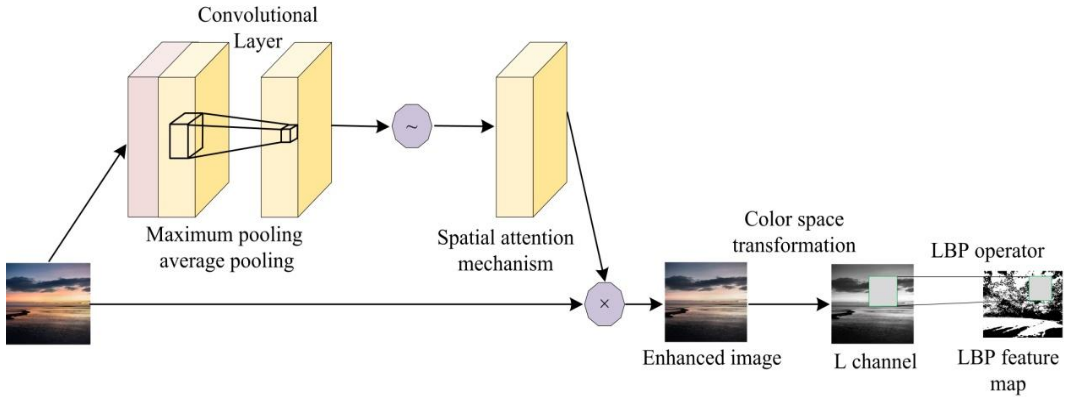

Figure 2. *Texture FE module*

$$F'(F_{RGB}) = F_{RGB} \times \sigma\Big(f\big(\big[f_{avg}(F_{RGB}); f_{\max}(F_{RGB})\big]\big)\Big) \tag{Eq.1}$$

In *Equation (1)*, F_{RGB} represents the original features of the image. $\sigma(\cdot)$ represents the activation function. $f_{avg}(\cdot)$ represents average pooling. $f(\cdot)$ represents convolution operation. $f_{\max}(\cdot)$ represents maximum pooling. The color space transformation module can convert the color space of the target image, avoiding the extraction of color information in the texture FE module. The texture information features extracted after color space conversion are used as inputs for the LBP operator, and the conversion formula is shown in *Equation (2)* (Li and Khan, 2023; Wang and Zheng, 2023).

$$F_L = f_{lab}\big([R, G, B]\omega\big) \tag{Eq.2}$$

In *Equation (2)*, $f_{lab}(\cdot)$ represents the method of calculating the brightness index in Lab space through XYZ space. F_L represents image features that do not contain color information. (ω) represents the conversion matrix from RGB space to XYZ space. The LBP operator has grayscale invariance and can reduce the interference of uneven lighting on model accuracy. This method calculates the LBP features of the surrounding area based on the central pixel point, as shown in *Equation (3)*.

$$F_{LBP} = \sum_{i=0}^{p}\Big(G(g_i - g_c)2^{i-1}\Big) \tag{Eq.3}$$

In *Equation (3)*, $G(\cdot)$ is the sign function. g_i is the pixel value of sampling point. F_{LBP} represents the LBP features of the surrounding area of a pixel. The sign function is shown in *Equation (4)*.

$$G(g_i - g_c) = \begin{cases} 0, & g_i - g_c > 0 \\ 1, & g_i - g_c \le 0 \end{cases} \tag{Eq.4}$$

http://www.aloki.hu ● ISSN 1589 1623 (Print) ● ISSN 1785 0037 (Online)
DOI: http://dx.doi.org/10.15666/aeer/2401_353374

This method can effectively reduce background interference in the surrounding areas of the park landscape. The final thousand layer module extracted by the texture color dual branch FE module is shown in *Equation (5)*.

$$F_T = f_{\max}\left(\left[f\left(F_{RGB}\right); f\left(F_{LBP}\right)\right]\right) \tag{Eq.5}$$

In *Equation (5)*, F_T represents the output of the texture color dual branch FE module. F_{RGB} represents the input color feature information. F_{LBP} represents the texture feature information of the input. In summary, the dual branch FE module for texture and color is shown in *Figure 3*.

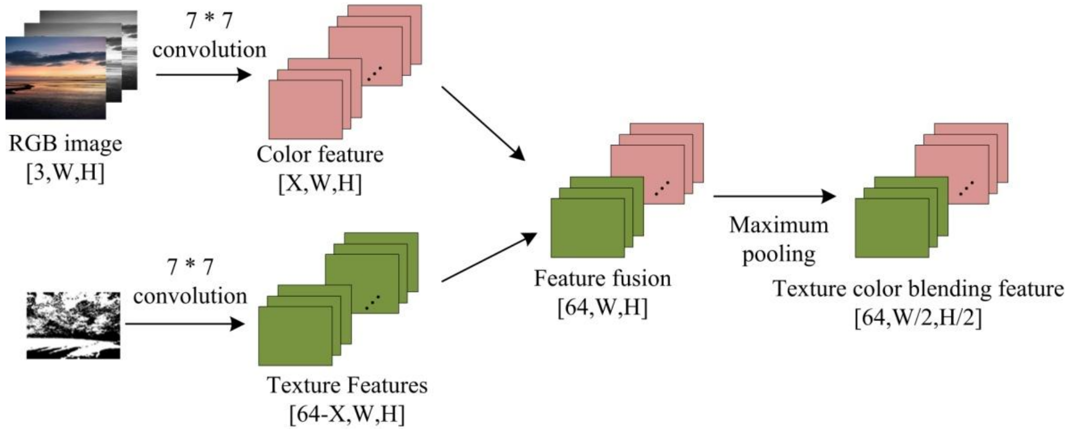

Figure 3. *Texture color dual branch FE module*

As shown in *Figure 3*, the multi-scale residual shrinkage module (MRS-block), a cornerstone of the improved architecture, consists of two cascaded multi-scale residual modules. The features of the target area are extracted and denoised through the MRS-block module. The MRS-block module can adaptively adjust FE for FE at different scales during FE. The structure of the multi-scale shrinkage residual module is shown in *Figure 4*.

As shown in *Figure 4*, the MRS-block consists of a bottleneck structure, a multi-scale FE module, and a residual shrinkage module. Through multi-scale convolution, residual connection, and soft thresholding, it effectively extracts park landscape features. The residual linking method in this module is shown in *Equation (6)*.

$$H(x) = x + S\left(I(x)\right) \tag{Eq.6}$$

In *Equation (6)*, x represents the input of the multi-scale residual shrinkage module. $S(\cdot)$ represents residual shrinkage operation. $H(x)$ represents residual linking operations. $I(\cdot)$ represents multi-scale convolution FE. In the multi-scale FE module designed for research, an improved Inception module is introduced, which uses convolutions with different receptive fields for FE, as shown in *Equation (7)*.

$$I(x) = Concat\left\{f^{1\times1}(x), f^{3\times3}(x), f^{5\times5}(x), f_{avg}(x)\right\} \tag{Eq.7}$$

http://www.aloki.hu ● ISSN 1589 1623 (Print) ● ISSN 1785 0037 (Online)
DOI: http://dx.doi.org/10.15666/aeer/2401_353374

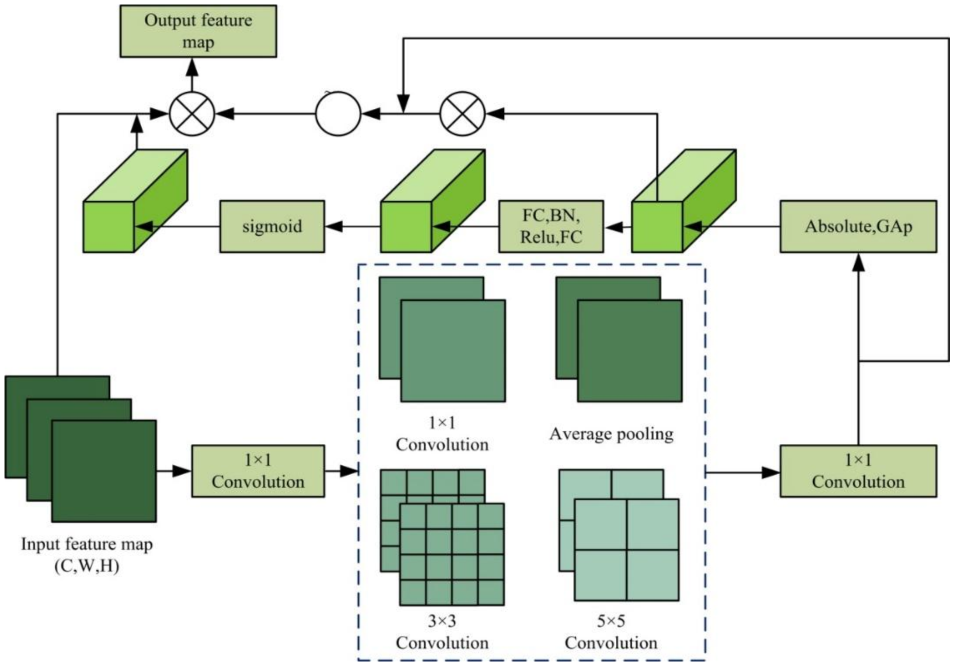

***Figure 4.** Multi-scale contraction residual module structure*

In *Equation (7)*, $f^{i\times j}(x)$ represents the convolution operation for different receptive fields. $Concat\{\cdot\}$ represents the linking operation of multi-scale features. A bottleneck layer is added before the FE output structure to reduce computational parameters (Franke and Peter, 2023). The bottleneck layer of the research design filters the output feature structure through 1×1 convolution after each branch input, reducing computational parameters and generating multi-scale features, as shown in *Equation (8)*.

$$x' = f^{1\times1}\left(f^{1\times1}\left(I(x)\right)\right) \tag{Eq.8}$$

In FE, the shrinkage module first takes the absolute value of the input feature map and globally pools it to obtain a new feature map, thereby achieving the shrinkage of the target feature, as shown in *Equation (9)*.

$$F_{gap} = \frac{1}{H\times W}\sum_{i=1}^{H}\sum_{j=1}^{W}\left|x'_{i,j,C}\right| \tag{Eq.9}$$

In *Equation (9)*, F_{gap} represents the globally pooled feature map. After obtaining the new feature map, it is input into a fully connected sub network composed of two 1×1 convolutions and sigmoid functions to obtain normalized scaling parameters, and then obtain a threshold. The input multi-scale feature map is processed according to the threshold, as shown in *Equation (10)*.

$$S(x',t) = \begin{cases} x'-t, & x' > t \\ 0, & -t \le x' \le t \\ x'+t, & x' < -t \end{cases} \tag{Eq.10}$$

http://www.aloki.hu ● ISSN 1589 1623 (Print) ● ISSN 1785 0037 (Online)
DOI: http://dx.doi.org/10.15666/aeer/2401_353374

In *Equation (10)*, t represents the threshold. The feature processing pipeline involves removing features with absolute values below a predefined threshold, shrinking features with absolute values exceeding the threshold toward zero, thereby reducing information redundancy, suppressing background noise, and enhancing the edge and texture features of the park landscape. The residual shrinkage structure is mainly based on attention mechanism, combined with soft thresholding mechanism, which enhances the attention mechanism to distinguish similar structural features in the image through soft thresholding mechanism, thereby improving the anti-interference level of the amplifier (Alsekait et al., 2024). After being processed by the residual shrinkage module, the connection between different channels can be adaptively learned between different levels, thereby outputting the recognition results of urban park landscape categories.

Urban thermal environment prediction based on CA-Markov

After extracting and analyzing the landscape features of urban parks in the target area, the thermal environment of the target area can be predicted and analyzed to investigate the relationship between urban park landscape and thermal environment. Before conducting predictive analysis of urban thermal environment, it is necessary to preprocess experimental data (Shao et al., 2023; Aman and Bhaskar, 2024). The data used in the experiment is remote sensing data from Landsat series satellites. To ensure the model captures the most recent and relevant urban development dynamics, the CA-Markov model was trained and validated using a multi-year dataset of Landsat-8/9 satellite images from 2018 to 2023. This six-year period provides a robust temporal foundation, effectively capturing the key trends and transition probabilities of the urban thermal environment necessary for reliable short-to-mid-term forecasting. Before using these data for temperature inversion and thermal environment prediction, preprocessing of the data is required, as shown in *Figure 5*.

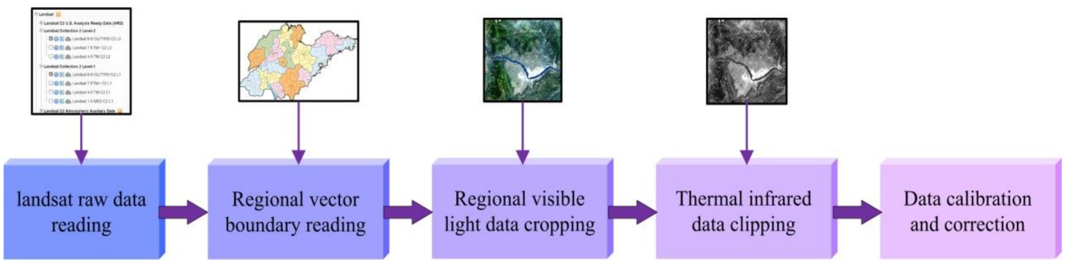

Figure 5. *Remote sensing data preprocessing process*

According to *Figure 5*, the data preprocessing steps include image cropping, radiometric calibration, and atmospheric correction. Image cropping is the process of cropping an image for each band, extracting the study area from the entire image to reduce post-processing computational complexity (Sunesh et al., 2023). Radiometric calibration is the process of converting satellite recorded data, which mainly relies on sensor gain. By offsetting the satellite observation value DN, numerical conversion is achieved, as shown in *Equation (11)*.

$$L_\lambda = gain \times DN + offset \tag{Eq.11}$$

In *Equation (11)*, $offset$ represents sensor offset. L_λ indicates the radiance value. Atmospheric correction is calculated using ENVI software by setting relevant parameters based on image information (Zhang et al., 2023; Dereich et al., 2024). To eliminate errors caused by factors such as atmosphere and lighting, and to make the results closer to the actual vegetation spectrum. The surface temperature can measure the energy within a city, and the surface temperature of the target area can be obtained through inversion method. The inversion method used in the study is the radiative transfer equation method, as shown in *Figure 6*.

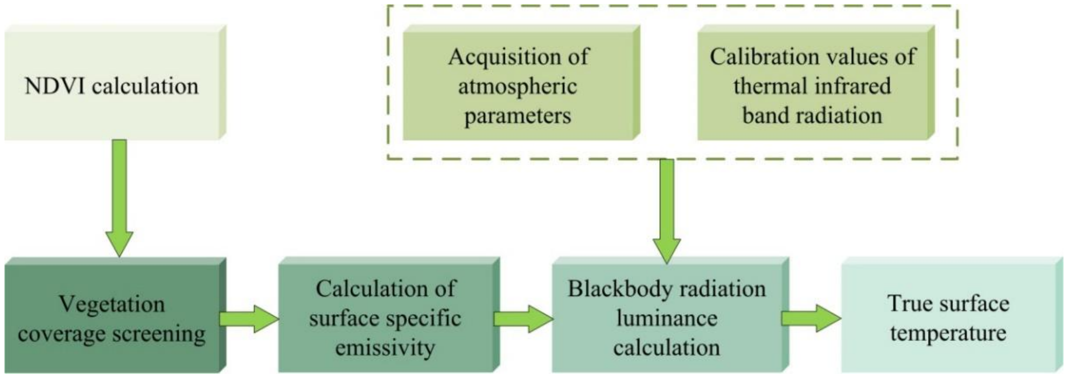

Figure 6. *Surface temperature inversion process*

As shown in *Figure 6*, during surface inversion, it is necessary to first calculate the Normalized Difference Vegetation Index (NDVI), input the corresponding band in ENVI software to automatically calculate NDVI, and select the confidence interval based on the actual NDVI value. Subsequently, vegetation coverage screening is conducted using mixed pixel decomposition method to distinguish different regions and present the vegetation coverage on the land surface as shown in *Equation (12)*.

$$Fv = \frac{NDVI - NDVI_s}{NDVI_v - NDVI_s} \quad \text{(Eq.12)}$$

In *Equation (12)*, Fv represents the preparation coverage. After determining the preparation coverage, the surface emissivity is estimated. The atmospheric profile parameters can be obtained on NASA's official website (Douandji et al., 2025). The calculation of surface temperature not only requires atmospheric parameters, but also the calculation of blackbody radiance, as shown in *Equation (13)*.

$$B(TS) = \frac{\left[L_\lambda - L\uparrow - \tau(1-\varepsilon)L\downarrow\right]}{\tau\varepsilon} \quad \text{(Eq.13)}$$

In *Equation (13)*, $B(TS)$ represents the blackbody thermal radiance. ε represents surface emissivity. $L\uparrow$ and $L\downarrow$ respectively represent the radiance of upward and downward atmospheric radiation. τ indicates the transmittance of the atmosphere in the thermal infrared band. TS represents the true surface temperature. After completing the inversion of surface temperature, the urban thermal environment can be predicted based

http://www.aloki.hu ● ISSN 1589 1623 (Print) ● ISSN 1785 0037 (Online)
DOI: http://dx.doi.org/10.15666/aeer/2401_353374

on the inversion results (Maurya et al., 2023). The CA-Markov model is mainly used to simulate the spatiotemporal evolution process of geographical features. Markov chain is based on historical state transition probabilities to predict the type transition probabilities at future time points. Cellular automata introduce spatial neighborhood rules to simulate the dynamic changes in spatial distribution. Therefore, the study uses this model to predict urban thermal environment, and the model framework is shown in *Figure 7*.

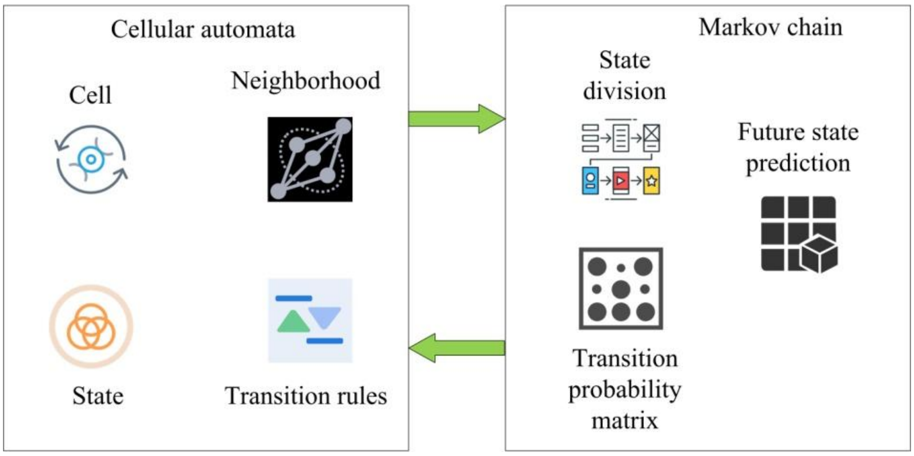

Figure 7. *CA-Markov model framework*

As presented in *Figure 7*, the CA-Markov model includes two parts: CA and Markov chain. The CA model is a discrete and dynamic model that is discrete in time, space, and state, with limited variable states. The core principle is that each cell interacts with its surrounding cells and changes over time according to specific transformation rules, which are localized in time and space and is capable of modeling the temporal-spatial dynamics of intricate systems. For example, in the simulation of urban heat island intensity (HII) levels, the cell size is consistent with the grid, and the HII level of the grid represents the cell state. The cell state is influenced by surrounding cells, and through interaction and conversion rules, the simulation of changes in HII levels is achieved. Markov model is a stochastic process model, Markov chain, which indicates that the probability distribution of a state at a certain moment depends only on the state at that moment and is independent of previous states. The CA model can simulate the spatial variation of HII levels, while the Markov model can calculate transition probabilities and areas. The CA-Markov model combines the two to simulate the intensity level changes of urban heat islands in space, reflect the influence of surrounding cells, and visually present their distribution status, greatly improving the accuracy and scientificity of simulation results.

Correlation analysis based on landscape pattern indices

To quantitatively analyze the correlation between park landscape characteristics and the urban thermal environment, a set of landscape pattern indices at both the class level and the landscape level were calculated. These indices were computed using FRAGSTATS software based on the land cover classification results obtained from the improved MSRN2 model and the thermal environment classification derived from the CA-Markov model prediction.

http://www.aloki.hu ● ISSN 1589 1623 (Print) ● ISSN 1785 0037 (Online)
DOI: http://dx.doi.org/10.15666/aeer/2401_353374

Class level indices were used to describe the spatial pattern of each thermal environment class (such as low temperature and high temperature zones). These indices include: (1) Area Perimeter Fractal Dimension (APFD), which is a measure of the complexity of patch shape. The higher the APFD value, the more complex and irregular the shape; (2) Large Patch Index (LPI), which is used to quantify the percentage of maximum patches in the total landscape area. High LPI indicates the dominant position of a single patch type in the landscape; (3) Patch density (PD), which defines the number of patches per unit area. PD reflects the degree of landscape fragmentation. The higher the PD, the more fragmented the landscape; (4) Edge density (ED), which measures the total length of all edge segments per unit area. The increase in ED indicates a higher degree of plaque fragmentation and interface.

Landscape level indices are used to describe the overall characteristics of thermal landscape tiling. These indices include: (1) Shannon Diversity Index (SHDI), which measures the diversity of patch types within the landscape. The higher the SHDI, the greater the diversity of thermal environment categories; (2) Contagious Index (CONTAG), which describes the degree of aggregation or clustering of plaque types. A high CONTAG value indicates that the landscape is dominated by continuous patches; (3) DIVISION, which refers to the degree of spatial separation between patches of the same type. The higher the value, the larger the division; (4) Shannon Uniformity Index (SHEI), whichrefers to the uniformity of area distribution between different patch types. SHEI is equal to SHDI divided by the maximum possible diversity of a given number of plaque types.

In addition, the Normalized Difference Vegetation Index (NDVI) is calculated during the surface temperature inversion process to estimate vegetation coverage. Although the main NDVI results are intermediate inputs for temperature inversion, the spatial distribution of NDVI values is analyzed to validate the extracted vegetation cover features within the park landscape.

Results

Analysis of the extraction effect of park landscape features

The research mainly focuses on Shanghai, located in the Yangtze River Delta region of eastern China (approximately 31°N, 121°E). The city belongs to the northern subtropical monsoon climate, with hot and humid summers and mild and relatively dry winters. A total of 27 major urban parks have been identified in the region, ranging in area from 2 hectares to 150 hectares. The park is composed of mixed vegetation such as broad-leaved trees, coniferous trees, and lawns. Non park areas are mostly impermeable surfaces, buildings of different heights, dense transportation networks, and scattered small green spaces. For landscape and thermal analysis, Landsat-8/9 satellite images from 2022 to 2023 were used. The spatial resolution of the multispectral band is 30 meters, while the inherent resolution of the thermal infrared band is 100 meters. To ensure consistency in analysis, bilinear interpolation was used to resample all thermal infrared data to a 30 meter resolution to match multispectral data. When verifying the effectiveness of the MSRN2 model in extracting landscape features of urban parks, a simulation testing platform was built, and *Table 1* presents comprehensive details.

On the simulation testing platform, the performance of the park landscape FE model was tested and analyzed, including FE accuracy, FE efficiency, FE loss, and model convergence. The convergence of the model and the loss of FE are shown in *Figure 8*.

http://www.aloki.hu ● ISSN 1589 1623 (Print) ● ISSN 1785 0037 (Online)
DOI: http://dx.doi.org/10.15666/aeer/2401_353374

Table 1. *Detailed information of simulation testing platform*

Name	Type	Name	Type
GPU	NVIDIA RTX 4090	CPU	AMD Ryzen Threadripper PRO
Operating system	Ubuntu 22.04 LTS	Driver version	NVIDIA Driver 535+
Dependent libraries	Python 3.10+	Data management	PostgreSQL 15 + PostGIS 3.3
Auxiliary tools	Jupyter Lab 4.0	CA-Markov Model Tool	IDRISI TerrSet 2023
GIS	QGIS 3.32 / ArcGIS Pro 3.1	Deep learning framework	PyTorch 2.0+

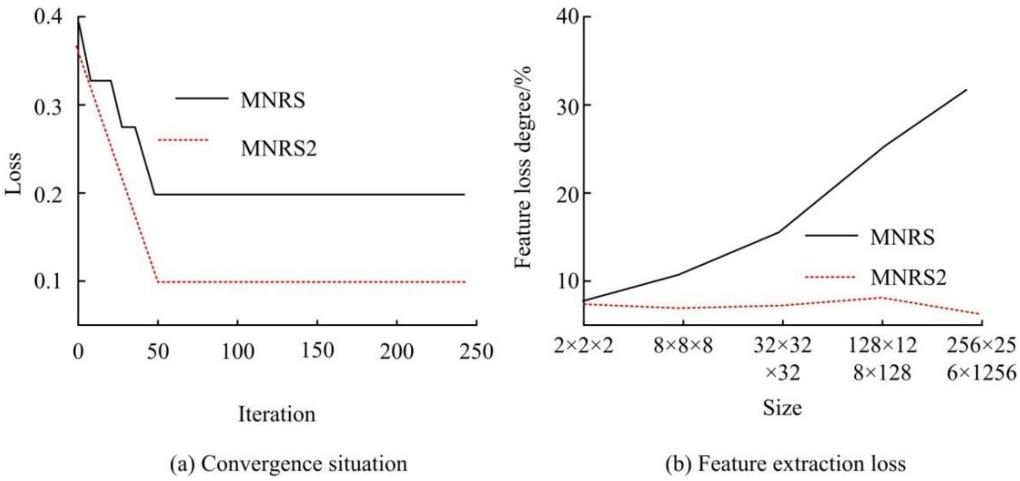

Figure 8. *The convergence of FE models and the degree of FE loss*

Figure 8(a) shows the convergence of the FE model. The MNRS model completed convergence after 50 iterations, and the loss value of model convergence remained around 0.2. The MNRS2 model designed for research converged after 30 iterations, and the loss value of the model after convergence remained around 0.15. The convergence speed of the research design model was faster under the same conditions, and the loss degree after convergence is smaller. Compared to traditional FE models, the iterative training effect of research model was better. *Figure 8(b)* shows the image FE loss of the FE model. In the FE process of the MNRS model, the loss of image features increased with the increase of input images. The larger the input image, the greater the feature loss of the model. When the input size increased to 256×256×256, the feature loss of the model reached 32.3%. The MNRS2 model maintained a feature loss of less than 5% during the FE process. The research model had a high sensitivity to small image features. The FE accuracy and efficiency of the two models are shown in *Figure 9*.

Figure 9(a) shows a comparison of the extraction accuracy of two models. The MNRS model maintained an FE accuracy of around 0.85 during the testing process, with the highest reaching 0.91 and the lowest reaching 0.82. During the testing process, the FE accuracy of the MNRS2 model remained above 0.95, with a maximum of 0.98. The accuracy test results of FE showed that the improved MNRS model had a good FE effect in urban park landscape FE, and could effectively distinguish the features of park landscape from other areas. *Figure 9(b)* shows a comparison of FE efficiency between

http://www.aloki.hu ● ISSN 1589 1623 (Print) ● ISSN 1785 0037 (Online)
DOI: http://dx.doi.org/10.15666/aeer/2401_353374

two models. As the input images of the models increased, the FE efficiency of both models gradually decreased. When the input image was small, the FE efficiency of the two models was basically the same. When the input image was increased to 256×256×256, it took 132 seconds for the MNRS model to complete FE, and 53 seconds for the MNRS2 model to complete FE. The research model had higher FE accuracy, less time required, and higher efficiency. The model was used to extract features from urban remote sensing images, and Figure 10 illustrates the findings.

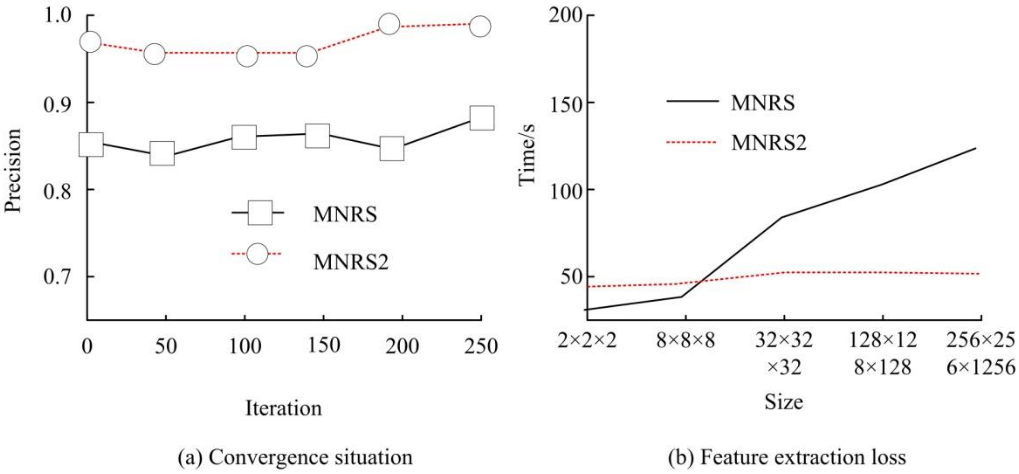

Figure 9. *Comparison of accuracy and efficiency of FE models*

Figure 10 shows the FE results when the classification category was 2. The image was divided into two categories, which could roughly distinguish the two relatively obvious types of land features in the city, but there was a lot of detail loss, unable to accurately distinguish between buildings with different functions or different vegetation types in green spaces. *Figure 10(b)* shows the FE results when the classification category was 3. After increasing the number of categories to 3, the model could distinguish more types of land features. *Figure 10(c)* shows the FE results when the classification category was 4. When the number of categories reached 4, the classification became more detailed and could present more details of land features. It may be possible to distinguish buildings of different materials or uses, as well as more accurately delineate areas such as green spaces and water bodies. The results demonstrated that increasing the number of classification categories could automatically improve the characterization of land features by providing more granular and discriminative details. However, it is important to note that while a higher number of categories enhanced feature differentiation, it might also lead to overly fragmented classifications and increase computational complexity and analytical overhead. As the number of categories increased, the image displayed more detailed information and could distinguish more different types of land cover, but it may also lead to overly detailed classification and increase the complexity of analysis.

Analysis of the prediction effect of urban thermal environment

The CA-Markov model was employed to simulate and predict the urban heat situation of X city in 2023, and the outcomes are presented in *Figure 11*. The model was first rigorously validated by simulating the known thermal environment of 2023. The results demonstrated a high degree of consistency with the actual situation, with an overall

http://www.aloki.hu ● ISSN 1589 1623 (Print) ● ISSN 1785 0037 (Online)
DOI: http://dx.doi.org/10.15666/aeer/2401_353374

prediction error of less than 5%, confirming the model's effectiveness and suitability for forecasting. *Figure 11(a)* indicates the actual urban heat of X city in 2023, and *Figure 11(b)* shows the simulation outcomes of the CA-Markov model. Through the analysis of different levels of HII, the error between low temperature (LT) and HT zones was relatively large. This indicated that the simulation accuracy for LT and HT areas was relatively low during the simulation process, which may be due to the influence of various complex factors on these two areas. For example, LT areas may be affected by terrain, vegetation coverage, and other factors, while HT areas may be affected by urban construction, population density, and other factors, resulting in greater simulation difficulty. From the overall view in the figure, the outcomes revealed no substantial discrepancy between the actual situation and the simulated situation in the study area in 2023, indicating that the simulation of the HII in X city grounded in the CA-Markov model had certain reliability and could reflect the actual distribution of HII to a certain extent.

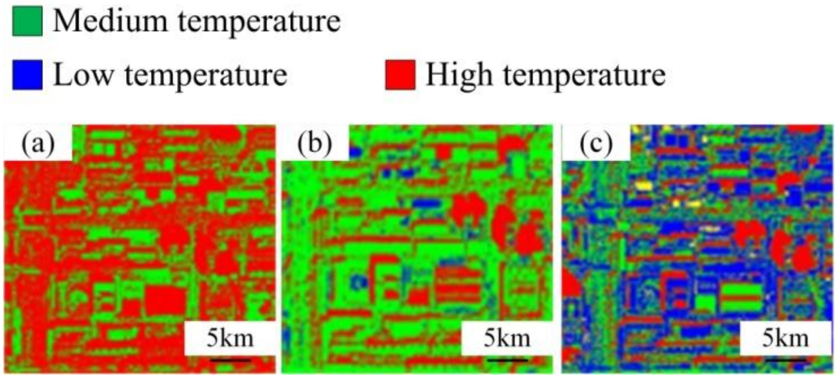

***Figure 10.** FE of urban remote sensing images*

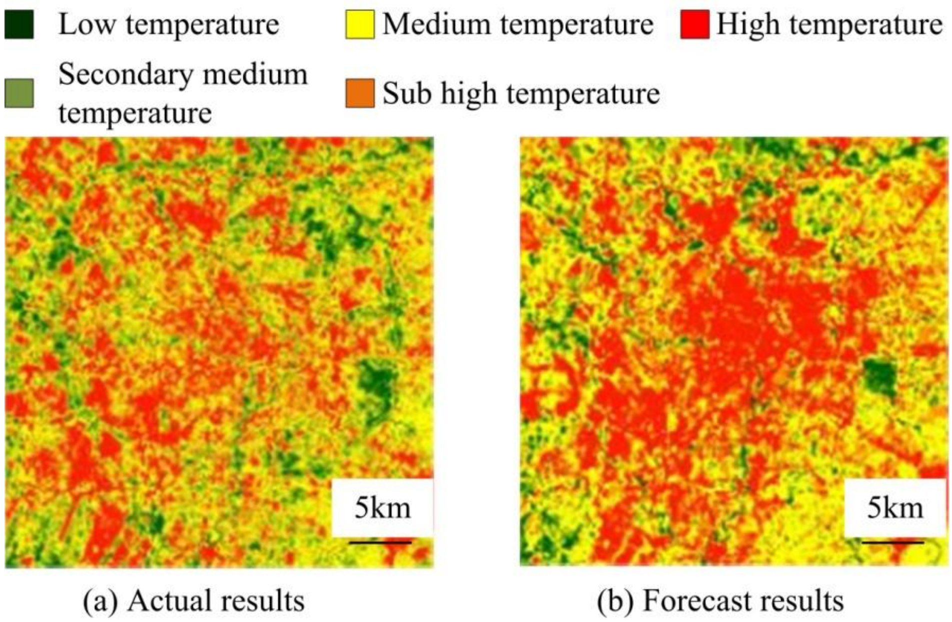

***Figure 11.** Simulation and prediction results of urban heat*

http://www.aloki.hu ● ISSN 1589 1623 (Print) ● ISSN 1785 0037 (Online)
DOI: http://dx.doi.org/10.15666/aeer/2401_353374

The study further predicted the urban thermal environment of X city in 2030 and 2035, and compared it with the thermal environment of X city in 2023.These projections were based on the well-validated model and revealed clear and consistent trends, such as the significant expansion of high-temperature areas, which provided valuable insights for urban planning. The proportion of different temperature zones was analyzed, and the outcomes are presented in *Table 2*.

Table 2. *Prediction of thermal environment in X city by 2030*

Index	LT zone	Sub moderate temperature zone	Medium temperature zone	Sub HT zone	HT zone
2030 predicted number of pixels	551239	704574	1524549	558645	742393
Predicted proportion of pixels in 2030 (%)	14.31	17.28	34.39	10.74	22.52
2035 predicted number of pixels	551225	704308	1524432	558989	742509
Predicted proportion of pixels in 2035 (%)	14.28	16.82	33.74	13.43	24.98
Actual proportion in 2023 (%)	14.28	17.98	37.37	13.82	16.79
Growth rate from 2023 to 2030 (%)	0.03	-0.70	-2.98	-3.08	5.73
Growth rate from 2023 to 2035	0	1.16	-3.63	-0.39	8.19

In 2030, the proportion of medium temperature area in the research area was the highest, accounting for 34.39%, while the proportion of sub HT area was the lowest, accounting for 10.74%. This indicated that in the predicted future thermal environment, the medium temperature zone still accounted for a significant proportion of the thermal landscape in the study area, but decreased to a certain extent compared to 2018. The proportion of sub HT zones was consistently low and showing a downward trend. Overall, the proportion of medium and sub HT areas decreased, while the proportion of HT areas significantly increased, indicating an increasing trend of urban HIE and the continuous expansion of HT areas. Based on the changes in the proportion of intensity levels of various heat islands, the heat island phenomenon in the study area would be difficult to alleviate in the short term in the future. The ongoingexpansion in the region of HT zones would lead to increasingly serious urban thermal environment problems, exerting greater pressure on the urban ecological environment, residents' lives, and sustainable development.

Correlation analysis between park landscape and urban thermal environment

When analyzing the connection between park landscape and urban thermal environment, the landscape pattern index of different thermal regions was studied and analyzed. The landscape pattern index was indicated by four basic indicators. The APFD was used to measure plaque transformation, and a higher index corresponded to a greater degree of complexity in the plaque shape. The LPI was used to measure whether a patch was a dominant patch. The larger the LPI, the more likely the patch was to be a dominant patch, and its changes could reflect the ramifications of human actions upon the patch. The Patch Density Index (PDI) was used to measure the number of heat island level patches and also to assess the degree of thermal environment fragmentation in the region. The smaller the PDI index, the fewer the number of urban heat islands, and the lower the degree of damage to the urban heat island environment. Edge density of plaques (EDP) was used to measure the degree of plaque fragmentation, and an increase in the index corresponded to a greater degree of plaque fragmentation. The landscape pattern index results of X city from 2019 to 2024 are shown in *Figure 12*.

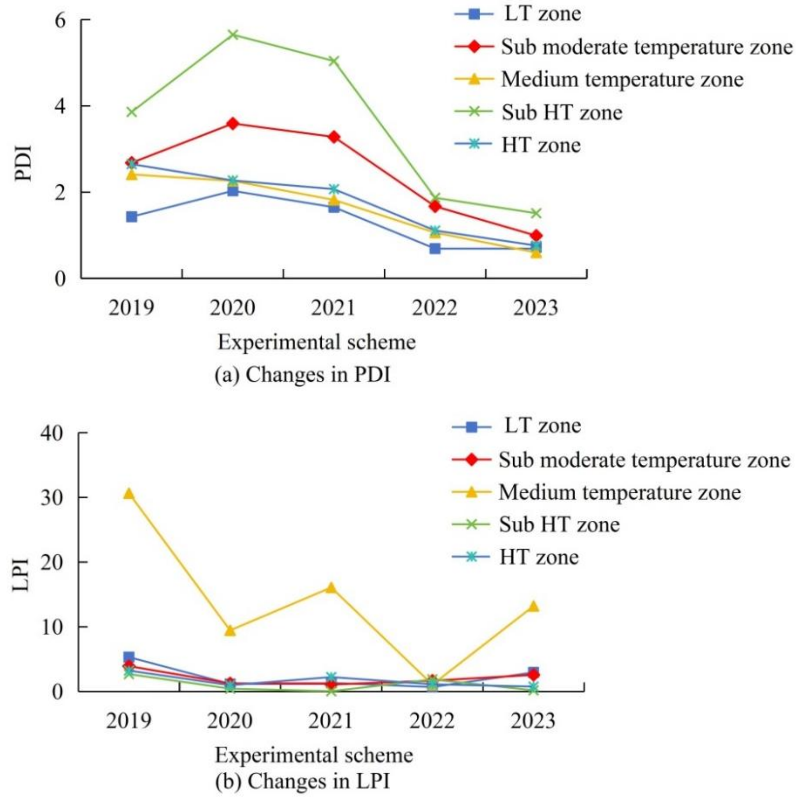

Figure 12. *Change of landscape pattern index in X City*

Figure 12(a) indicates the changes in PDI, and *Figure 12(b)* indicates the changes in LPI. The PDI in the sub HT zone was usually the highest, and the degree of landscape differentiation was high. However, the overall PDI of various thermal levels showed a downward trend, and landscape fragmentation was reduced and tended to cluster. The LPI in the temperate zone was always high and was a dominant plaque, but its value gradually decreased and its dominance weakened. The study further analyzed the landscape level index, which was indicated by four indicators. The Diversity Index (DI) reflected the heterogeneity of thermal landscapes and was sensitive to the distribution of patch types at different levels of HII. The Contag Index (CI) was used to measure the spread of different thermal landscapes in urban heat island environments. The Separation Index (SI) measured the degree of dispersion of different patches within a landscape,

http://www.aloki.hu ● ISSN 1589 1623 (Print) ● ISSN 1785 0037 (Online)
DOI: http://dx.doi.org/10.15666/aeer/2401_353374

ranging from 1 to the square of the total number of grids. An increase in the value led to a higher degree of patch dispersion. The Uniformity Index (UI) was equal to the Shannon Diversity Index divided by the maximum possible diversity given landscape abundance. The landscape level index results of X city from 2019 to 2024 are shown in *Figure 13*.

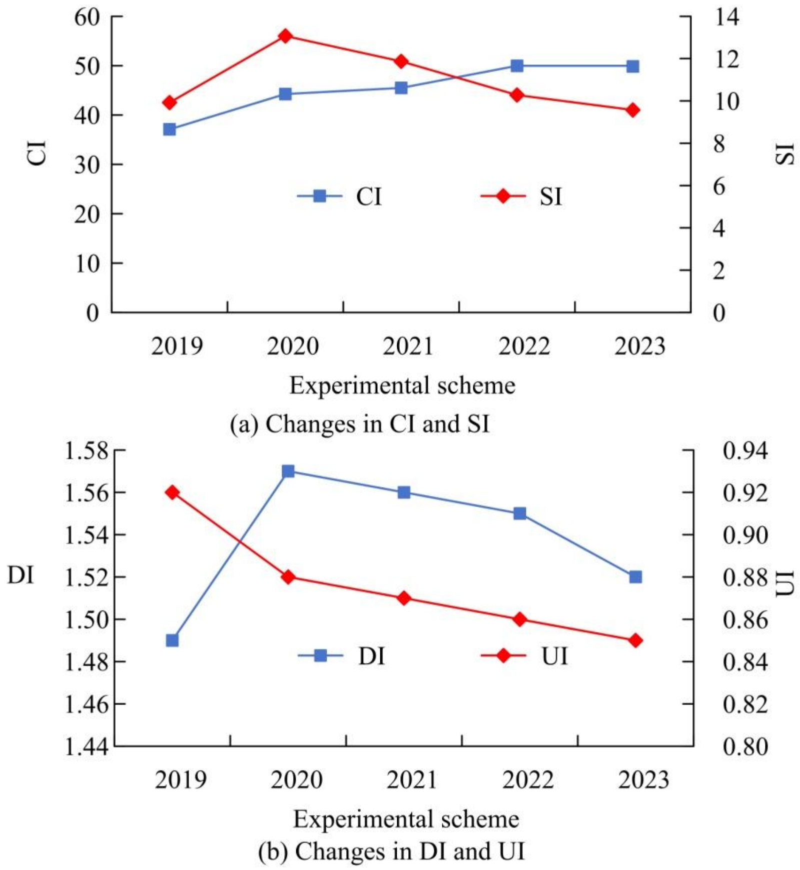

Figure 13. *Landscape level index results*

Figure 13(a) shows the changes inSI and CI, while *Figure 13(b)* shows the changes inDI and UI. The CI steadily climbed from 37.10 to 49.79. This was due to the integration and aggregation of various patches in the process of urban construction. HT patches gradually dominated in this process, and the trend of thermal landscape aggregation would become increasingly evident in the future. Although this reduced landscape fragmentation to a certain extent, it may also lead to the concentration of HT areas, exacerbating the urban HIE. The SI increased from 9.92 to 13.07, reflecting a heterogeneous distribution of thermal landscapes and an increase in the degree of dispersion between patches. As time went by, the separation degree of different levels of thermal patches gradually decreased, the degree of patch fragmentation decreased, and the connection between various types of thermal patches gradually strengthened, which was conducive to the diffusion of heat. The overall trend of DI was on the rise, and the proportion of thermal landscape types gradually increased towards HT areas. The diversification of landscape types decreased, and the impact of HT areas on urban thermal environment became increasingly significant. The UI showed a downward trend, and the spatial distribution of hot landscapes would become even more uneven in the future.

Discussion

The study systematically explored the correlation between urban park landscape and thermal environment by integrating improved MSRN2 algorithm and CA-Markov model. The experimental results showed that the proposed method exhibited significant advantages in FE accuracy, prediction reliability, and landscape thermal environment correlation analysis.

Firstly, the improved MSRN2 algorithm significantly enhanced its ability to capture multi-scale features of urban park landscapes by introducing a texture color dual branch FE module and attention mechanism. Its FE accuracy of up to 0.98 and efficiency improvement of about 60% verified the effectiveness of the model in handling highly heterogeneous landscape elements in complex urban environments. Especially by introducing the LBP Transformer hybrid module in the texture branch, not only did it enhance sensitivity to local textures, but it also improved the model's overall understanding of landscape structures through a global attention mechanism, which was relatively rare in previous methods based on a single convolutional network.

Secondly, the CA Markov model showed strong reliability in predicting the spatiotemporal evolution of urban thermal environment, with an overall error of less than 5%, especially in high-temperature areas where the prediction error was only 1.66%. This indicated that the model could simulate the spatial diffusion trend of urban HIE well, providing a practical tool for medium and long-term thermal environment assessment. However, the model had relatively high errors in low-temperature and high-temperature regions, which might be related to the greater influence of non-landscape factors in these areas. In the future, more socio-economic or meteorological data can be considered to enhance the explanatory power of the model.

In terms of correlation analysis, the changes in landscape pattern index revealed a significant positive correlation between park landscape fragmentation and expansion in high-temperature areas. With the advancement of urbanization, the landscape aggregation degree (CONTAG) increased while the SHDI decreased, indicating that the urban thermal environment is becoming more homogeneous and centralized, and high-temperature patches are gradually dominating the urban thermal landscape. This finding is consistent with existing research on the important role of green space continuity in mitigating the HIE, further confirming the potential value of optimizing park spatial layout in improving urban thermal environment.

The research findings of this article emphasize the significant correlation between landscape pattern indices and the expansion of high-temperature regions at the macro spatial scale, consistent with the systematic review by El-Metwally et al. (2025). Their comprehensive analysis of the Kopen climate zone emphasizes that the configuration and spatial pattern of urban green spaces are universal key factors affecting their cooling effect, which is a fundamental premise strongly supported by our quantitative model (El-Metwally et al., 2025). However, although the macro and model driven methods of research and design are helpful for city wide planning, they have not captured the detailed human centered fine scale thermal comfort dynamics described in Zhan and Wang (2025) work. Their research on waterfront parks in Zhengzhou has revealed how specific design elements directly affect human thermal comfort, providing a valuable direction for future research. In addition, our study identified the aggregation of high-temperature patches as a key trend, which is consistent with the focus on the cooling effect of vegetation configuration. Nie et al. (2024) worked in temperate continental climate zones and demonstrated that specific plant community structures, such as tree shrub grass

http://www.aloki.hu ● ISSN 1589 1623 (Print) ● ISSN 1785 0037 (Online)
DOI: http://dx.doi.org/10.15666/aeer/2401_353374

combinations, have superior cooling benefits. This indicates the limitations of our current finite element model, which effectively identifies "green spaces" as a category but does not differentiate between internal vegetation structure or species composition (Nie et al., 2024).

In summary, the proposed improved MSRN2 algorithm combined with CA-Markov model provides an effective tool for quantitative correlation analysis between urban thermal environment and green landscape, and also provides a scientific basis for future smart city ecological planning and urban heat island mitigation strategies.

Conclusion

The research aimed to improve deep learning algorithms and prediction models to deeply analyze the correlation between urban park landscapes and thermal environments, providing scientific basis for optimizing green space allocation and mitigating the HIE. The research method proposed an improved MSRN2 algorithm, which enhanced the dynamic fusion ability of multi-source remote sensing data through a texture color dual branch FE module and attention mechanism. It combined CA-Markov model to predict the spatiotemporal evolution of urban thermal environment, and quantified the correlation between the two through landscape pattern index. Findings from the experiment demonstrated that the improved MSRN2 algorithm achieved a maximum FE accuracy of 0.98, with an efficiency improvement of about 60% compared to traditional models. Crucially, the CA-Markov model demonstrated high predictive reliability, with an overall error of less than 5% and a notably low error of 1.66% in the high-temperature zone. This validation confirmed the model's efficacy for forecasting thermal environment dynamics. Statistical assessment revealed a robust relationship between the decrease in fragmentation of park landscapes and the significant expansion of HT areas, indicating that the urban HIEwas continuously intensifying. Research confirmed that optimizing the spatial layout of park landscapes could effectively alleviate urban thermal environment problems and provide quantitative decision support for green space planning. However, there are still certain limitations to the research: Firstly, the data relied on Landsat remote sensing images, and the resolution limited the capture of micro landscape features. In the future, it will be necessary to integrate drone or high-resolution satellite data. Future research will focus on multi-source data fusion, model generalization ability improvement, and multi-scale environmental collaborative analysis to expand the application prospects of this paradigm in smart city ecological governance.

Fundings. The research is supported by: General Project of Philosophy and Social Sciences Research in Universities in Jiangsu Province, Research on the Integration of Culture and Tourism and Rural Revitalization under the Path of Art Intervention (No. 2023SJYB1914).

REFERENCES

[1] Abdelkarim, A. (2025): Monitoring and forecasting of land use/land cover (LULC) in Al-Hassa oasis, Saudi Arabia based on the integration of the cellular automata (CA) and the cellular automata-Markov model (CA-Markov). – Geology, Ecology, and Landscapes 9(1): 13-44. https://doi.org/10.1080/24749508.2022.2163741.

[2] Alsekait, D., Zakariah, M., Amin, S. U., Khan, Z. I., Alqurni, J. S. (2024): Privacy preservation in IoT devices by detecting obfuscated malware using wide residual network. – Computers, Materials and Continua 81(2): 2395-2436. https://doi.org/10.32604/cmc.2024.055469.
[3] Aman, G., Bhaskar, D. (2024): Enhancing the city-level thermal environment through the strategic utilization of urban green spaces employing geospatial techniques. – International Journal of Biometeorology 68(10): 2083-2101. https://doi.org/10.1007/s00484-024-02733-2.
[4] Atef, I., Ahmed, W., AbdelMaguid, R. H. (2024): Future land use land cover changes in El-Fayoum governorate: a simulation study using satellite data and CA-Markov model. – Stochastic Environmental Research and Risk Assessment 38(2): 651-664. DOI: 10.1007/s00477-023-02592-0.
[5] Bian, R. (2024): Landscape painting style transfer and feature extraction model based on convolutional neural networks. – International Journal of Multiphysics 18(2): 581-599.
[6] Chen, M., Feng, D., Zhang, S., Jiang, Y., Zhang, X. (2023): Dynamic monitoring and prediction of eco-environmental quality in Yining city based on RSEI and ANN-CA-Markov model. – Arid Land Geography 46(6): 911-921. DOI: 10.12118/j.issn.1000-6060.2022.446.
[7] Chen, S., Huang, Y., Tan, D., Wang, J., Qi, H., Zhang, H., Su, Z., Wang, Y. (2025): Prediction and spatial driving force analysis of soil erosion in Badong county based on CA-Markov model. – Science Soil Water Conservence 23(1): 222-232. DOI: 10.16843/j.sswc.2024065.
[8] Dereich, S., Jentzen, A., Kassing, S. (2024): On the existence of minimizers in shallow residual ReLU neural network optimization landscapes. – SIAM Journal on Numerical Analysis 62(6): 2640-2666. DOI:10.1137/23M1556241.
[9] Douandji, F. M. D., Kamga, B. Y., Ndumbe, L. N., Nkondjoua, A. D. T., Ngoh, M. L., Nguetsop, V. F. (2025): Land use/land cover dynamics and future changes using a CA-Markov model in the mount Nlonako forest and peripheries (littoral, Cameroon). – Journal of Geoscience and Environment Protection 13(2): 230-260. DOI: 10.4236/gep.2025.132015.
[10] El-Metwally, Y., Elshater, A., Fahmy, M., Elrahman, A. S. A., Alwaer, H., Elbardisy, W. M. (2025): Assessing the impact of urban parks across Köppen climatic zones: A systematic review. – Proceedings of the Institution of Civil Engineers – Urban Design and Planning 178(1): 6-20. https://doi.org/10.1680/jurdp.23.00049.
[11] Franke, L., Peter, C. (2023): Visualizing the residue interaction landscape of proteins by temporal network embedding. – Journal of Chemical Theory and Computation 19(10): 2985-2995. https://doi.org/10.1021/acs.jctc.2c01228.
[12] Gloire, K. S., Vami Hermann, N. B., Fernand, K. K. (2023): Analysis and prediction of the mode of land use based on the combined use of the Dempster-Shafer evidence theory model and the CA-Markov model: application to the buildings of the city of Goma in the Democratic Republic of the Congo. – Revue Francaise de Photogrammetrie et de Télédétection 225(1): 24-36.
[13] Hou, M., Chen, Y., Cao, S., Chen, Y., Ying, J. (2023): HRW: hybrid residual and weak form loss for solving elliptic interface problems with neural network. – Numerical Mathematics Theory Methods and Applications 16(4): 883-913.
[14] Hu, J., Geng, G., Xiong, M., Li, S., Zhang, Y. (2025): A style transfer method for Chinese landscape painting based on detail feature extraction and fusion. – Advanced Engineering Sciences 57(1): 98-106.
[15] Jayabaskaran, M., Das, B. (2023): Land use land cover (LULC) dynamics by CA-ANN and CA-markov model approaches: a case study of Ranipet town, India. – Nature Environment and Pollution Technology 22(3): 1251-1265. DOI:10.46488/NEPT.2023.v22i03.013.

[16] Kisamba, F. C., Li, F. (2023): Analysis and modelling urban growth of Dodoma urban district in Tanzania using an integrated CA-Markov model. – GeoJournal 88(1): 511-532. https://doi.org/10.1007/s10708-022-10617-4.

[17] Lewandowski, B., Paffenroth, R. (2023): Autoencoder feature residuals for network intrusion detection: one-class pretraining for improved performance. – Machine Learning & Knowledge Extraction 5(3): 868-890. https://doi.org/10.3390/make5030046.

[18] Li, W. (2023): Texture feature extraction of a landscape design image based on the contour wave transform. – International Journal of Data Science 8(1): 39-51. DOI:10.1504/IJDS.2023.129456.

[19] Li, P., Khan, J. (2023): Feature extraction and analysis of landscape imaging using drones and machine vision. – Soft Computing 27(24): 18529-18547. https://doi.org/10.1007/s00500-023-09352-w.

[20] Luan, Y., Huang, G., Zheng, G. (2023): Spatiotemporal evolution and prediction of habitat quality in Hohhot city of China based on the inVEST and CA-Markov models. – Journal of Arid Land 15(1): 20-33. https://doi.org/10.1007/s40333-023-0090-8.

[21] Maurya, N. K., Rafi, S., Shamoo, S. (2023): Land use/land cover dynamics study and prediction in Jaipur city using CA-Markov model integrated with road network. – Geojournal 88(1): 137-160. https://doi.org/10.1007/s10708-022-10593-9.

[22] Mustaquim, M., Islam, W. (2025): Analysing land use and cover transformations in Berhampore, west Bengal, India: a CA-Markov and ANN simulation approach for future predictions. – Agricultural Research 14(1): 171-187. https://doi.org/10.1007/s40003-024-00745-3.

[23] Nie, X., Lin, J., Ma, J., Cao, B., Li, Y., Lu, Y., Bian, Y., Liu, J., Zhang, P. (2024): The cooling effect of plant configuration on urban parks green space in temperate continental climate zones. – Applied Spatial Analysis 17(4): 1463-1483. https://doi.org/10.1007/s12061-024-09590-x.

[24] Pouriyeh, A. (2023): Identification and prediction of land use changes based on artificial neural network and CA-Markov for sustainable land-use planning. – International Journal of Global Warming 30(4): 349-366. https://doi.org/10.1504/IJGW.2023.132272.

[25] Said, Y., Alassaf, Y., Saidani, T., Ghodhbani, R., Rhaiem, O. B., Alalawi, A. A. (2024): Context-aware feature extraction network for high-precision UAV-based vehicle detection in urban environments. – Computers, Materials & Continua 81(3): 4349-4370. https://doi.org/10.32604/cmc.2024.058903.

[26] Satalkar, V., Degaga, G. D., Li, W., Pang, Y. T., McShan, A. C., Gumbart, J. C., Mitchell, J. C., Torres, M. P. (2024): Generative b-hairpin design using a residue-based physicochemical property landscape. – Biophysical Journal 123(17): 2790-2806. https://doi.org/10.1016/j.bpj.2024.01.029.

[27] Shao, J. Q., Qian, W. H., Xu, Q. H. (2023): Landscape image generation based on conditional residual generative adversarial network. – Journal of Graphics 44(4): 710-717.

[28] Simon, O., Lyimo, J., Yamungu, N. (2023): Land use and cover change in dar es salaam metropolitan city: satellite data and CA-Markov chain analysis. – Geojournal 88(6): 6119-6136. https://doi.org/10.1007/s10708-023-10960-0.

[29] Solaimani, K., Darvishi, S. (2024): Comparative analysis of land use changes modeling based on new hybrid models and CA-Markov in the Urmia lake basin. – Advances in Space Research 74(8): 3749-3764. https://doi.org/10.1016/j.asr.2024.06.078.

[30] Sunesh, N. P., Indran, S., Divya, D., Suchart, S. (2023): Extraction and physico-mechanical and thermal characterization of a novel green bio-plasticizer from *Pedalium murex* plant biomass for biofilm application. – Journal of Polymers and The Environment 31(10): 4353-4368. https://doi.org/10.1007/s10924-023-02898-8.

[31] Wang, S., Zheng, X. (2023): Dominant transition probability: combining CA-Markov model to simulate land use change. – Environment, Development and Sustainability 25(7): 6829-6847. https://doi.org/10.1007/s10668-022-02337-z.

[32] Zhan, J., Wang, N. (2025): Study on the relationship between summer microclimate and human thermal comfort in urban waterfront parks-Longzi Lake Park in Zhengzhou city as an example. – Landscape and Ecological Engineering 21(2): 341-356. https://doi.org/10.1007/s11355-025-00644-x.

[33] Zhang, Q., Zhang, J., Lu, S., Liu, Y., Liu, L., Wang, Y., Cao, M. (2023): Multi-resolution feature extraction and fusion for traditional village landscape analysis in remote sensing imagery. – Traitement du Signal 40(3): 1259-1266. DOI:10.18280/ts.400344.

[34] Zui, H. (2024): The concept of core feature parameter of geographic information to cultural landscape genes of traditional settlements. – Journal of Geo-information Science 26(4): 989-1001. DOI: 10.12082/dqxxkx.2024.230743.